Inorg. Chem. **2005**, *44*, 3311–3320

Copper–Zinc Superoxide Dismutase: Theoretical Insights into the Catalytic Mechanism

Vladimir Pelmenschikov* and Per E. M. Siegbahn

Department of Physics, Stockholm University, S-106 91 Stockholm, Sweden

Received January 6, 2005

The mechanism for the toxic superoxide radical disproportionation to molecular oxygen and hydrogen peroxide by copper–zinc superoxide dismutase (CuZnSOD) has been studied using the B3LYP hybrid density functional. On the basis of the X-ray structure of the enzyme, the molecular system investigated includes the first-shell protein ligands of the two metal centers as well as the second-shell ligand Asp122. The substrates of the model reaction are two superoxide radical anions, approaching the copper center at the beginning of two half-reactions: the first part of the catalytic cycle involving Cu^{+} oxidation and the second part reducing Cu^{2+} back to its initial state. The quantitative free energy profile of the reaction is obtained and discussed in connection with the experimental data on the reduction potentials and CuZnSOD kinetics. The optimized structures are analyzed and compared to the experimental ones. The two transition states alternate the protonation state of His61 and correspond to histidine Cu-His61-Zn bridge rupture/reformation. Modifications applied to the initial model allow the importance of Asp122 for catalysis to be estimated.

I. Introduction

In metabolism of aerobes, the superoxide radical anion $O_2^{\bullet-}$ is encountered via one-electron reduction of molecular oxygen. As an intermediate or occasional byproduct during respiration or photosynthesis and as an immune response product of phagocytes during respiratory burst,[1,2] the superoxide radical is very toxic. Along with hydrogen peroxide (H_2O_2) and the hydroxyl radical ($^{\bullet}OH$), superoxide has been implicated in oxidative damage phenomena related to aging, inflammation, and postischemic injury via reperfusion. To provide cellular defense against the oxidative stress, nature utilizes superoxide dismutases (SODs), catalyzing $O_2^{\bullet-}$ disproportionation into the less toxic dioxygen and hydrogen peroxide:

$$2O_2^{\bullet-} + 2H^{+} \xrightarrow{\text{SOD}} O_2 + H_2O_2 \qquad (1)$$

So far, three unrelated kinds of SODs have been characterized, all being metalloenzymes. The classes have been classified depending on their active site metal ion content: Cu- and Zn-dependent SODs (CuZnSODs); SODs that use Fe, Mn, or either of the two (FeSODs, MnSODs, or Fe/MnSODs); and Ni-dependent enzymes (NiSODs).

Among SODs, copper- and zinc-containing enzymes are probably the most abundant, found in all eucaryotes and many procaryotes. Point mutations in CuZnSOD are linked to 20% of the cases of familial amyotrophic lateral sclerosis (FALS),[3−5] a fatal neurodegenerative disease leading to paralytic disorder. CuZnSOD, earlier known as "erythrocuprein", was the first natural $O_2^{\bullet-}$ scavenger identified.[6] CuZnSOD in eucaryotes is a 2×16 kDA homodimer with one copper and one zinc per subunit (see Figure 1). Each subunit features a flattened eight-stranded antiparallel "greek-key" β-barrel tertiary structure.[7,8] The distance between the two active sites in the homodimer is over 30 Å, so that the subunits probably act independently during catalysis.[9] Available sequencies of the CuZnSOD family reveal strictly conserved residues in the active site region (see Figure 2). The structural His44, His46, and His118 ligands coordinate copper, and His69, His78, and Asp81 coordinate zinc. The metal ions are separated by about 6 Å, and His61 plays an exceptional bridging role coordinating copper by N^{ϵ}_{His61} and zinc by N^{δ}_{His61}. The Asp122 carboxylate provides additional

* Author to whom correspondence should be addressed. E-mail: vovan@physto.se.

(1) Fridovich, I. *J. Biol. Chem.* **1989**, *264*, 7761−7764.
(2) Fridovich, I. *J. Exp. Biol.* **1998**, *201*, 1203−1209.
(3) Rosen, D. R.; Siddique, T.; Patterson, D.; Figlewicz, D. A.; Sapp, P.; Hentati, A.; Donaldson, D.; Goto, J.; O'Regan, J. P.; Deng, H. X. *Nature* **1993**, *362*, 59−62.
(4) Stathopulos, P. B.; Rumfeldt, J. A.; Scholz, G. A.; Irani, R. A.; Frey, H. E.; Hallewell, R. A.; Lepock, J. R.; Meiering, E. M. *Proc. Natl. Acad. Sci. U.S.A.* **2003**, *100*, 7021−7026.
(5) Liochev, S. I.; Fridovich, I. *Free Radical Biol. Med.* **2003**, *34*, 1383−1389.
(6) McCord, J. M.; Fridovich, I. *J. Biol. Chem.* **1969**, *244*, 6049−6055.
(7) Tainer, J. A.; Getzoff, E. D.; Beem, K. M.; Richardson, J. S.; Richardson, D. C. *J. Mol. Biol.* **1982**, *160*, 181−217.
(8) Tainer, J. A.; Getzoff, E. D.; Richardson, J. S.; Richardson, D. C. *Nature* **1983**, *306*, 284−287.

10.1021/ic050018g CCC: $30.25
Published on Web 04/07/2005

Figure 1. Tertiary structure of the reduced bovine CuZnSOD homodimer, complexed with azide (PDB code 1SXZ).[27] Cu^{+} and Zn^{2+} ions are given as light and dark spheres, respectively, and important active site residues together with the azide N_3^- bound to Cu^{+} are shown. The picture was generated using VMD 1.8.2 molecular visualization program.[71] See Figure 2 for a more detailed picture of the active site.

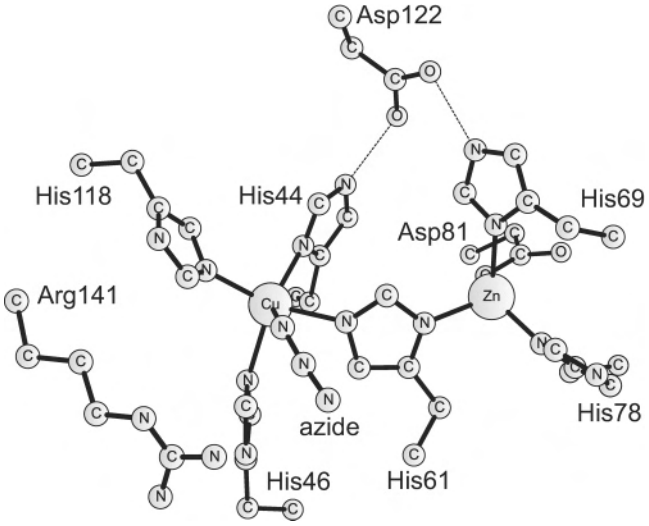

Figure 2. Active site of the reduced Cu^{+} bovine CuZnSOD, complexed with azide (PDB code 1SXZ).[27] Bovine erythrocyte amino acid sequence numbering is used here.

stabilization of the dinuclear metal cluster, forming an indirect bridge via hydrogen bonding to both N^{ϵ}_{His44} and N^{ϵ}_{His69}. The positive guanidino group of Arg141 is located within 5 Å of copper and has been proposed[10−14] to play an important role in the local electrostatic attraction of $O_2^{\bullet-}$ anions by providing a superoxide docking site, as described below. The rest of the conserved residues[9] (not shown) are involved in maintaining the proper conformation of the enzyme (Gly80, Gly136, Cys55-S-S-Cys144 disulfide bridge) and electrostatic steering of the superoxide anions into the active site cleft (Lys120, "electrostatic triad" Asp130, Glu131, and Lys134). CuZnSODs (as well as NiSODs) are known as superefficient $O_2^{\bullet-}$ scavengers with second-order ($k_2^{CuZnSOD} = k_{cat}/K_M$) catalytic rates as high as 10^9-10^{10} M^{-1} s^{-1},[10,14] as compared to the second-order rate of the uncatalyzed reaction ($k_2^{uncat} \approx 2 \times 10^5$ M^{-1} s^{-1}) at neutral pH.[2] Under substrate saturation conditions, $k_{cat} \approx 1 \times 10^6$ s^{-1} and $K_M \approx 3 \times 10^{-3}$ M^{-1} were obtained for the bovine isoenzyme.[15] Under nonsaturating conditions, the rate-limiting process in the dismutation is the diffusion of $O_2^{\bullet-}$ anions toward the active site cavity, and electrostatic guidance here plays a key role.[10,16] A net positive electrostatic potential near the reactive center of superefficient SODs probably contributes to the substrate binding.[17] In *Escherichia coli*, only 5[18] of the superoxide radicals evade from dismutation by SOD. With its concentration in aerobic cells normally at the [SOD] $\approx 10^{-5}$ M^{-1} level, this enzyme keeps the steady-state superoxide concentration at $[O_2^{\bullet-}] \approx 10^{-10}$ M^{-1}.[19,20] For a given $O_2^{\bullet-}$ molecule, the probability to meet a molecule of SOD is thus much higher than it is to meet another $O_2^{\bullet-}$. Taking into account this concentrational factor, SOD in the cellular environment shortens the lifetime of the superoxide radical by a factor of $k_2^{CuZnSOD}/k_2^{uncat} \times [SOD]/[O_2^{\bullet-}] \approx 10^{10}$.

A set of small anions can penetrate into the active site and inhibit the enzyme. The cavity opening is approximately 24 Å across at the enzymes surface, and the dead end of the channel is as narrow as 4 Å. The active site is terminated at the copper ion, which is partly exposed to the solvent. Cyanide (CN^-), azide (N_3^-) (see Figures 1 and 2), and fluoride (F^-) can bind directly to copper; iodide (I^-) and somewhat more bulky anions such as phosphate (PO_3^{2-}) remain at the Arg141 guanidino site.[21] The Zn^{2+} ion is completely blocked from solution and cannot accept extra ligands, thus playing only an indirect role in catalysis. Beside its structural function in coordinating N^{δ}_{His61} of the bridging

(9) Bordo, D.; Pesce, A.; Bolognesi, M., E.; S. M.; Falconi, M.; Desideri, A. In *Handbook of Metalloproteins*, Vol. 2; Messerschmidt, A., Huber, R., Poulos, T. L., Wieghardt, K., Eds.; Wiley & Sons: Chichester, 2001.
(10) Getzoff, E. D.; Tainer, J. A.; Weiner, P. K.; Kollman, P. A.; Richardson, J. S.; Richardson, D. C. *Nature* **1983**, *306*, 287−290.
(11) Bannister, J. V.; Parker, M. W. *Proc. Natl. Acad. Sci. U.S.A.* **1985**, *82*, 149−152.
(12) Beyer, W. F., Jr.; Fridovich, I.; Mullenbach, G. T.; Hallewell, R. *J. Biol. Chem.* **1987**, *262*, 11182−11187.
(13) Polticelli, F.; Battistoni, A.; O'Neill, P.; Rotilio, G.; Desideri, A. *Protein Sci.* **1998**, *7*, 2354−2358.
(14) Stroppolo, M. E.; Falconi, M.; Caccuri, A. M.; Desideri, A. *Cell. Mol. Life Sci.* **2001**, *58*, 1451−1460.
(15) Fee, J. A.; Bull, C. *J. Biol. Chem.* **1986**, *28*, 13000−13005.
(16) Koppenol, W. H. In *Oxygen and Oxyradicals in Chemistry and Biology*; Rodgers, M. A. J., Powers, E. L., Eds.; Academic Press: New York, 1981.
(17) Miller, A.-F. *Curr. Opin. Chem. Biol.* **2004**, *8*, 162−168.
(18) Liochev, S. I.; Fridovich, I. *Proc. Natl. Acad. Sci. U.S.A.* **1997**, *94*, 2891−2896.
(19) Imlay, J. A.; Fridovich, I. *J. Biol. Chem.* **1997**, *266*, 6957−6965.
(20) Ponderoso, J. J.; Lisdero, C.; Schopfer, F.; Riobo, N.; Carreras, M. C.; Cadenas, E.; Boveris, A. *J. Biol. Chem.* **1999**, *274*, 37709−37716.
(21) Hart, P. J.; Balbirnie, M. M.; Ogihara, N. L.; Nersissian, A. M.; Weiss, M. S.; Valentine, J. S.; Eisenberg, D. *Biochemistry* **1999**, *38*, 2167−2178.

histidine, Zn^{2+} has been shown to be important in electronic polarization and electrostatic stabilization.[22,23]

Structural analysis and spectroscopic studies reveal that an unprotonated imidazolate of the His61 bridge links copper and zinc in the cupric (Cu^{2+}) (oxidized) form of the enzyme. In the cuprous (Cu^{+}) (reduced) form, the N^{ϵ}_{His61} nitrogen becomes protonated and the Cu−His61-Zn bridge is lost at the copper side. Examination of the structures available shows a $Cu-N^{\epsilon}_{His61}$ distance typically varying around the two distinct values 2.2 and 3.0 Å.[9] In the recent, very high 1.15 Å resolution structure[24] of the reduced dimeric CuZnSOD, this distance is around 3.3 Å when averaged between the two subunits. There is however a set of reduced bovine CuZnSOD structures reported[25−27] with the $Cu-N^{\epsilon}_{His61}$ bond intact. One of these structures, complexed with an azide inhibitor and resolved to 2.05 Å, is shown in Figures 1 and 2. Azide is a competitive inhibitor to copper and likely to mimic the $O_2^{\bullet-}$ substrate binding.[21,27] In the absence of inhibitor anions, a water molecule weakly coordinated to copper is often found at the place of the azide. On the basis of NMRD[28] and mutagenesis[29] studies, it has been suggested that this water molecule is not important for the enzymatic reaction. The commonly accepted mechanism[8,9,21] has two steps, corresponding to the copper reduction and re-oxidation, as supported by pulse radiolysis experiments.[30,31] Accounting for the electrostatic repulsion, the two substrate $O_2^{\bullet-}$ molecules necessary for the dismutation as in eq 1 bind to the active site stepwise (the E acronym in eqs 2 and 3) symbolizes the enzyme ligand environment):

$$E\text{-}Cu^{2+}\text{-}N^{\epsilon-}_{His61}\text{-}E + O_2^{\bullet-} + H^+ \rightarrow E\text{-}Cu^{+} + H\text{-}N^{\epsilon}_{His61}\text{-}E + O_2 \quad (2)$$

$$E\text{-}Cu^{+} + H\text{-}N^{\epsilon}_{His61}\text{-}E + O_2^{\bullet-} + H^+ \rightarrow E\text{-}Cu^{2+}\text{-}N^{\epsilon}_{His61}\text{-}E + H_2O_2 \quad (3)$$

The first step in eq 2 follows the above-mentioned copper reduction and concomitant $Cu-N^{\epsilon}_{His61}$ bond protonation. The reduction is suggested to occur via inner sphere electron transfer with direct $O_2^{\bullet-}$ coordination to the Cu^{2+} metal center. The resulting Cu^{+} cuprous form then adopts a trigonal planar coordination.[24,32−33] The first product is O_2 which can easily diffuse out, since it is neutral of charge, allowing for the entrance of the successive substrate molecule. Before the existence of the reduced azide-bound CuZnSOD form (see Figure 2) had been demonstrated by X-ray crystallography, Fourier transform infrared spectroscopy (FTIR) analysis[34] had provided arguments against the direct coordination of the azide to the Cu^{+} center. Instead, the azide was predicted to bind at the Arg141 guanidino site. By analogy to azide binding, the second step in eq 3 was suggested to proceed via outer sphere electron transfer from Cu^{+} to $O_2^{\bullet-}$, with the superoxide molecule localized at Arg141. Copper should then re-oxidize to its initial Cu^{2+} cupric form, followed by Cu-His61-Zn bridge reformation and hydrogen peroxide product release through the proton donation from N^{ϵ}_{His61}. The protons required for the dismutation should come from solution.[15] The delivery of those protons could be facilitated by a chain of conserved hydrogen-bonded water molecules in the CuZnSOD active site channel.[21,24,35] To provide the driving force necessary for the dismutation in the two-step redox process of eqs 2 and 3, the metal reduction potential of SOD should fall between the reduction potentials of O_2 and $O_2^{\bullet-}$.[23,36,37] The experimental data on CuZnSOD $E^{\circ\prime}(Cu^{2+}/Cu^{+})$ forms a broad range from +120 to +420 mV[38−42] and satisfies the above condition, given $E^{\circ\prime}(O_2/O_2^{\bullet-}) = -160$ mV and $E^{\circ\prime}(O_2^{\bullet-}/H_2O_2) = +890$ mV ($E^{\circ\prime}$ values are given vs standard hydrogen electrode at 1 M, 25 °C, and pH ≈ 7).

Mutagenesis studies[12,43] show that the Arg141 → Ile modification of CuZnSOD is still 10% active, showing that Arg141 is important but not essential for the catalytic activity. In case the Arg141 modification affects k_{cat} only, 10% activity would correspond to a mechanism with an activation energy for the rate-limiting step 1.4 kcal/mol higher than for the wild-type enzyme. In the present context of finding the main origin of catalysis, this effect is considered rather small, and Arg141 was therefore left out of the model at this stage. On the basis of the present model, a mechanistic pathway for the dismutation in CuZnSOD is suggested. The role of Asp122 was then investigated via modifications of the initial model.

(22) Konecny, R.; Li, J.; Fisher, C. L.; Dillet, V.; Bashford, D.; Noodleman, L. *Inorg. Chem.* **1999**, *38*, 940−950.
(23) Noodleman, L.; Lovell, T.; Han, W.-G.; Li, J.; Himo, F. *Chem. Rev.* **2004**, *104*, 459−508.
(24) Hough, M. A.; Hasnain, S. S. *Structure* **2003**, *11*, 937−946.
(25) Banci, L.; Bertini, I.; Bruni, B.; Carloni, P.; Luchinat, C.; Mangani, S.; Orioli, P. L.; Piccioli, M.; Rypniewski, W.; Wilson, K. S. *Biochem. Biophys. Res. Commun.* **1994**, *202*, 1088−1095.
(26) Rypniewski, W. R.; Mangani, S.; Bruni, B.; Orioli, P. L.; Casati, M.; Wilson, K. S. *J. Mol. Biol.* **1995**, *251*, 282−296.
(27) Ferraroni, M.; Rypniewski, W. R.; Bruni, B.; Orioli, P.; Mangani, S. *J. Biol. Inorg. Chem.* **1998**, *3*, 411−422.
(28) Sette, M.; Bozzi, M.; Battistoni, A.; Fasano, M.; Paci, M.; Rotilio, G. *FEBS Lett.* **2000**, *483*, 21−26.
(29) Bertini, I.; Banci, L.; Luchinat, C.; Bielski, B. H. J.; Cabelli, D. E.; Mullenbach, G. T.; Hallewell, R. A. *J. Am. Chem. Soc.* **1989**, *483*, 714−719.
(30) Klug-Roth, D.; Fridovich, I.; Rabani, J. *J. Am. Chem. Soc.* **1973**, *95*, 2786−2790.
(31) Fielden, E. M.; Roberts, P. B.; Bray, R. C.; Lowe, D. J.; Mautner, G. N.; Rotilio, G.; Calabrese, L. *Biochem. J.* **1974**, *139*, 49−60.
(32) Bailey, D. B.; Ellis, P. D.; Fee, J. A. *Biochemistry* **1980**, *19*, 591−596.
(33) Murphy, L. M.; Strange, R. W.; Hasnain, S. S. *Structure* **1997**, *5*, 371−379.
(34) Leone, M.; Cupane, A.; Militello, V.; Stroppolo, M. E.; Desideri, A. *Biochemistry* **1998**, *37*, 4459−4464.
(35) Ogihara, N. L.; Parge, H. E.; Hart, P. J.; Weiss, M. S.; Goto, J. J.; Crane, B. R.; Tsang, J.; Slater, K.; Roe, J. A.; Valentine, J. S.; Eisenberg, D.; Tainer, J. A. *Biochemistry* **1996**, *35*, 2316−2321.
(36) Stein, J. P.; Fackler, J. P. J.; McClune, G. J.; Fee, J. A.; Chan, L. T. *Inorg. Chem.* **1979**, *18*, 3511−3519.
(37) Barrette, W. C. J.; Sawyer, D. T.; Fee, J. A.; Asada, K. *Biochemistry* **1983**, *22*, 624−627.
(38) Fee, J. A.; DiCorleto, P. E. *Biochemistry* **1973**, *12*, 4893−4899.
(39) Lawrence, G. D.; Sawyer, D. T. *Biochemistry* **1979**, *18*, 3045−3050.
(40) St. Clair, C. S.; Gray, H. B.; Valentine, J. S. *Inorg. Chem.* **1992**, *31*, 925−927.
(41) Azab, H. A.; Banci, L.; Borsari, M.; Luchinat, C.; Sola, M.; Viezzoli, M. S. *Inorg. Chem.* **1992**, *31*, 4649−4655.
(42) Verhagen, M. F.; Meussen, E. T.; Hagen, W. R. *Biochim. Biophys. Acta* **1995**, *1244*, 99−103.
(43) Fisher, C. L.; Cabelli, D. E.; Tainer, J. A.; Hallewell, R. A.; Getzoff, E. D. *Proteins* **1994**, *19*, 24−34.

II. Computational Details

All the calculations were done using the B3LYP[44−46] hybrid density functional. Open shell systems were treated using unrestricted DFT. Geometry optimizations were performed using a standard valence LACVP basis set as implemented in the Jaguar 5.5 program.[47] For the first- and second-row elements, LACVP implies a 6-31G double-ζ basis set. For the copper and zinc atoms, LACVP uses a nonrelativistic effective core potential (ECP),[48] where the valence part is essentially of double-ζ quality. Local minima were optimized using the Jaguar 5.5 program. Analytical Hessians (second derivatives of the energy with respect to the nuclear coordinates) and the corresponding transition states were obtained using the Gaussian 98 program.[49] Accurate single-point energies ($E_{\mathrm{LACV3P**}}$) were obtained using the LACV3P** basis set of triple-ζ quality, which has a larger valence basis set for copper and zinc. For the rest of the atoms LACV3P** implies 6-311G** basis set with a single set of polarization functions added. Contributions from solvent effects (E_{SOLV}) to the accurate energies were computed within the LACV3P** basis set for the gas-phase optimized geometries using a Poisson−Boltzmann solver[50,51] as implemented in Jaguar 5.5. The radius of the solvent probe molecule was set to 1.40 Å, corresponding to the water molecule. The dielectric constant of the protein was set to $\epsilon = 4$, in line with previous studies.[22] To consider the effect of a more polar active site environment on the reaction energetics (see section III.d), the solvation calculations were repeated with $\epsilon = 80$ (corresponding to water). The Mulliken spin populations reported below in the text and figures are based on self-consistent reaction field (SCRF) spin densities, calculated using the LACV3P** basis set and including corrections from induced solvent charges. Thermochemical contributions[52] to the energies are the internal thermal energy (E_{THERM}) (including the zero-point energy) and entropy ($-TS$), which were obtained for optimized structures at the normal temperature ($T =$ 298.15 K), based on the computed Hessians.

A separate comment should be given on the estimation of the entropy contributions to the relative energies along the potential energy surface. The gas-phase calculations for the substrate and products of the dismutation would overestimate the absolute entropy values. Precisely prior to binding and after release, the molecular species are confined within the narrow active site channel and can move freely only a very short distance. Translational entropy (S_{tr}) contribution to the molar entropy in this case can be approximated using the modified Sackur−Tetrode equation:[53]

$$S_{\mathrm{tr}} = R\left(\ln\frac{\upsilon_{\mathrm{f}}}{\Lambda^3} + \frac{5}{2}\right) \tag{4}$$

where R is the gas constant, Λ is the thermal de Broglie wavelength of a molecule, and υ_{f} is the free volume in which the center of mass of a molecule can move inside the cavity. For CuZnSOD, the diameter of the active site chamber is ∼4.0 Å (see section I). Taking into account the size of a reactant or product molecule, a simple estimate for the free volume would be a spherical cavity of 1.0 Å radius with impenetrable walls. For the superoxide radical, hydrogen peroxide, and dioxygen this leads to a TS_{tr} value of 5.4 kcal/mol, as compared to the calculated gas-phase 10.8−10.9 kcal/mol range. Rotational (S_{rot}) and vibrational (S_{vibr}) entropies contribute less significantly to the total entropy, as compared to S_{tr}. S_{rot} and S_{vibr} estimations for a molecule in the cavity are not straightforward, and calculated gas-phase values were used here.

The ultimate Gibbs free energies obtained with $\epsilon = 4$ for E_{SOLV} are discussed below, if not otherwise stated, and include the individual terms described above:

$$G = E_{\mathrm{LACV3P**}} + E_{\mathrm{SOLV}} + E_{\mathrm{THERM}} - TS \tag{5}$$

The individual contributions for particular states are listed in Table 1. Errors in the relative energies calculated using the scheme described above are usually within 3 kcal/mol and rarely exceed 5 kcal/mol.[54]

When discussing the free energy change (ΔG_{OOH}) required for the protonation of the $O_2^{\bullet-}$ superoxide radical anion in solution, the following evaluation was used:

$$\begin{aligned}\Delta G_{\mathrm{OOH}} &= -RT\ln\frac{[^{\bullet}\mathrm{OOH}]}{[\mathrm{O_2}^{\bullet-}]} = RT\left(\ln\frac{[\mathrm{H^+}][\mathrm{O_2}^{\bullet-}]}{[^{\bullet}\mathrm{OOH}]} - \ln[\mathrm{H^+}]\right)\\ &= RT\ln 10\left(\log_{10}\frac{[\mathrm{H^+}][\mathrm{O_2}^{\bullet-}]}{[^{\bullet}\mathrm{OOH}]} - \log_{10}[\mathrm{H^+}]\right)\\ &= RT\ln 10(\mathrm{pH} - \mathrm{p}K_{\mathrm{a}}(\mathrm{OOH}))\\ &= 1.36(7 - 4.8)\mathrm{kcal/mol} = 3.0\mathrm{kcal/mol}\end{aligned} \tag{6}$$

Table 1. Contributions to the Energies of the Reductive and Oxidative Half-Reactions, Relative to the Reactants **1** and **4** (kcal/mol)[a]

state	$E_{\mathrm{LACV3P**}}$	E_{SOLV} ($\epsilon = 4/80$)	E_{THERM}	$-TS$	ΔG_{OOH}	G ($\epsilon = 4/80$)
1	0.0	0.0/0.0	0.0	0.0[b]	0.0	0.0/0.0
1′	−6.2	2.7/4.3	1.1	7.2	3.0	7.8/9.4
TS1	−0.1	1.2/2.4	−1.8	10.3	3.0	12.6/13.7
2	−27.4	1.5/2.2	3.0	1.6	3.0	−18.4/−17.7
3	−28.9	7.3/10.4	1.3	−2.0[b]	3.0	−19.3/−16.2
4	0.0	0.0/0.0	0.0	0.0[b]	0.0	0.0/0.0
5	−24.0	−0.4/0.5	1.7	8.3	3.0	−11.5/−10.6
TS2	−5.0	−1.6/1.4	−0.6	10.4	3.0	6.1/6.4
6′	−13.1	−2.4/−2.6	0.6	9.4	3.0	−2.5/−2.7
6	−6.1	−4.4/−5.6	−0.3	2.9[b]	3.0	−4.9/−6.2

[a] The total Gibbs free energies (G) are calculated according to eq 5, adding the ΔG_{OOH} correction due to pH factor, see section II and the second paragraph of section III.b. The free energy profile for $\epsilon = 4$ is also given in Figure 11. [b] Translational contributions to these entropy values were calculated according to the approximation in eq 4.

(44) Becke, A. D. *Phys. Rev. A* **1988**, *38*, 3098−3100.
(45) Becke, A. D. *J. Chem. Phys.* **1993**, *98*, 1372.
(46) Becke, A. D. *J. Chem. Phys.* **1993**, *98*, 5648.
(47) Schrödinger, L. L. C. *JAGUAR 5.5*; Portland, OR, 2003.
(48) Hay, P.; Wadt, W. *J. Chem. Phys.* **1985**, *82*, 299−310.
(49) Frisch, M. J.; Trucks, G. W.; Schlegel, H. B.; Scuseria, G. E.; Robb, M. A.; Cheeseman, J. R.; Zakrzewski, V. G.; Montgomery, J. A., Jr.; Stratmann, R. E.; Burant, J. C.; Dapprich, S.; Millam, J. M.; Daniels, A. D.; Kudin, K. N.; Strain, M. C.; Farkas, O.; Tomasi, J.; Barone, V.; Cossi, M.; Cammi, R.; Mennucci, B.; Pomelli, C.; Adamo, C.; Clifford, S.; Ochterski, J.; Petersson, G. A.; Ayala, P. Y.; Cui, Q.; Morokuma, K.; Malick, D. K.; Rabuck, A. D.; Raghavachari, K.; Foresman, J. B.; Cioslowski, J.; Ortiz, J. V.; Stefanov, B. B.; Liu, G.; Liashenko, A.; Piskorz, P.; Komaromi, I.; Gomperts, R.; Martin, R. L.; Fox, D. J.; Keith, T.; Al-Laham, M. A.; Peng, C. Y.; Nanayakkara, A.; Gonzalez, C.; Challacombe, M.; Gill, P. M. W.; Johnson, B. G.; Chen, W.; Wong, M. W.; Andres, J. L.; Head-Gordon, M.; Replogle, E. S.; Pople, J. A. *Gaussian 98*; Gaussian, Inc.: Pittsburgh, PA, 1998.
(50) Tannor, D.; Marten, B.; Murphy, R.; Friesner, R.; Sitkoff, D.; Nicholls, A.; Honig, B.; Ringnalda, M.; Goddard, W., III. *J. Am. Chem. Soc.* **1994**, *116*, 11875−11882.
(51) Marten, B.; Kim, K.; Cortis, C.; Friesner, R.; Murphy, R.; Ringnalda, M.; Sitkoff, D.; Honig, B. *J. Phys. Chem.* **1996**, *100*, 11775−11788.
(52) McQuarrie, D.; Simon, J. *Molecular Thermodynamics*; University Science Books: Sausalito, CA, 1999.
(53) Amzel, L. M. *Proteins* **1997**, *28*, 144−149.
(54) Siegbahn, P. *Q. Rev. Biophys.* **2003**, *36*, 91−145.

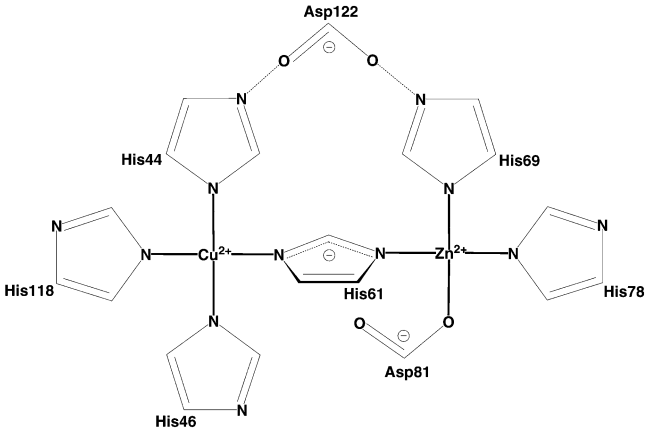

Figure 3. CuZnSOD active site model used in this study. Hydrogens are omitted for clarity.

where the experimental pK_a(OOH) = 4.8 for the hydroperoxyl (hydrogen dioxide, hydrodioxyl, or perhydroxyl) •OOH radical[55] was used.

The free energy change associated with the electron-transfer reactions is calculated from the Nernst equation:

$$\Delta G^{\circ\prime} = -nF\Delta E^{\circ\prime} \quad (7)$$

where n is the number of electrons exchanged in the process, $F = 23.06$ kcal mol^{-1} V^{-1} is the Faraday constant, and $\Delta E^{\circ\prime}$ is the corresponding electromotive force.

III. Results and Discussion

III.a. Chemical Models. The present modeling of the CuZnSOD active site is based on the X-ray structure of the reduced Cu^+ bovine enzyme, complexed with azide (PDB code 1SXZ)[27] (see Figures 1 and 2). In view of the mechanistic proposals (see section I), Cu and His61 are the key chemical species needed to be accurately modeled. Arg141 was not considered in our study in accordance with the arguments given above. Both the copper and zinc ions were included with all their ligands (His44,46,61,69,78,118 and Asp81). Asp122 is also present in the model. (The role for Asp122 is considered in section III.c.) The side chains of the residues included were truncated, with their β-carbons substituted by hydrogens. The structural histidines were thus modeled by imidazoles, and aspartates were modeled by formates. This type of modeling has been shown to be appropriate based on previous DFT studies of various enzymes[54] and is very similar to the modeling applied earlier by Konecny et al.[22] in their DFT study of CuZnSOD. The entire system in its Cu^{2+} oxidized resting state with the Cu-His61-Zn imidazolate bridge intact is shown schematically in Figure 3. The total charge of the system is +1 unit, and Cu^{2+} gives rise to a doublet spin state before the radical substrate arrival. No solvent water ligand is present at copper because it is displaced on substrate binding and its binding enthalpy to Cu^{2+} is small (only a few kcal/mol according to our calculations). As mentioned in section I, this water molecule is not likely to participate in the enzymatic reaction.

To reproduce the protein strain and a realistic positioning of the different chemical units, specific restrictions on some nuclear coordinates are sometimes applied. This is important in modeling fragments not directly bound to the metal.[56,57] In case of the system in Figure 3, this concerns only Asp122. However, the aspartate carboxylate forms hydrogen bonds to N^{ϵ}_{His44} and N^{ϵ}_{His69} in all the optimized structures and even provides an additional stabilization to the cluster when the Cu-His61-Zn bridge becomes protonated. Therefore, no fixations of nuclear coordinates were done during the geometry optimization in this study.

III.b. Dismutation Mechanism. Before discussing the presently suggested mechanism (see Figure 4) in detail, it is necessary to introduce one important approximation employed here. When the $O_2^{\bullet-}$ substrate radical penetrates into the active site channel and approaches the metal center, it can be protonated on its way by a proton donor, similarly as recently proposed for NiSOD.[58] Alternatively, CuZnSOD can provide a sufficiently low local pH in the vicinity to the catalytic center to stabilize the protonated superoxide radical. Stability of the local pH conditions can be supported by observations on the wild-type enzyme catalytic rate, which follows a pattern of a fairly constant value at pH 5−8.[30,59] The local delivery of protons and superoxides to copper is therefore postulated to be tightly linked, and the immediate substrate at the copper site is considered as an •OOH neutral radical.

Unified delivery of $O_2^{\bullet-}$ and H^+ is a notable simplification from the modeling point of view. This simplification means that no charge combination processes need to be modeled, which can be very difficult using the present type of relatively small molecular system. Those processes are, for example, very sensitive to the choice of dielectric constant. An additional advantage with the present type of modeling is that it is not necessary to consider any explicit source of the protons. In case the local pH inside the active site is not sufficiently low, this simplification of the modeling requires an energy correction. Using pK_a(OOH) = 4.8, the estimated cost to protonate $O_2^{\bullet-}$ at pH = 7 is 3.0 kcal/mol (see section II). Within the same mechanism as in Figure 4, a relative correction of −3.0 kcal/mol is therefore added to the energy of the states involving •OOH radicals (namely, **1** and **4**), to reference them to the true reactants ($O_2^{\bullet-} + H^+$).

i. Reductive Phase and O_2 Formation. The reductive phase includes states **1**-**3** in Figure 4 and starts from the oxidized Cu^{2+} state with the Cu-His61-Zn imidazolate bridge intact. An attempt to find an initial state **1′** with the hydroperoxyl substrate binding to copper at this point did not lead to metal reduction and $^-$OOH hydroperoxide anion formation. The local minimum found shows a very long copper to oxygen distance of 2.62 Å (see the Supporting

(55) Bielski, B. H. J.; Cabelli, D. E.; Arudi, R. L.; Ross, A. B. *J. Phys. Chem. Ref. Data* **1985**, *14*, 1041−1100.
(56) Pelmenschikov, V.; Siegbahn, P. E. M. *J. Biol. Inorg. Chem.* **2003**, *8*, 653−662.
(57) Pelmenschikov, V.; Cho, K.-B.; Siegbahn, P. E. M. *J. Comput. Chem.* **2004**, *25*, 311−321.
(58) Wuerges, J.; Lee, J.-W.; Yim, Y.-I.; Yim, H.-S.; Kang, S.-O.; Carugo, K. D. *Proc. Natl. Acad. Sci. U.S.A.* **2004**, *101*, 8569−8574.
(59) Fisher, C. L.; Cabelli, D. E.; Hallewell, R. A.; Beroza, P.; Lo, T. P.; Getzoff, E. D.; Tainer, J. A. *Proteins* **1997**, *29*, 103−112.

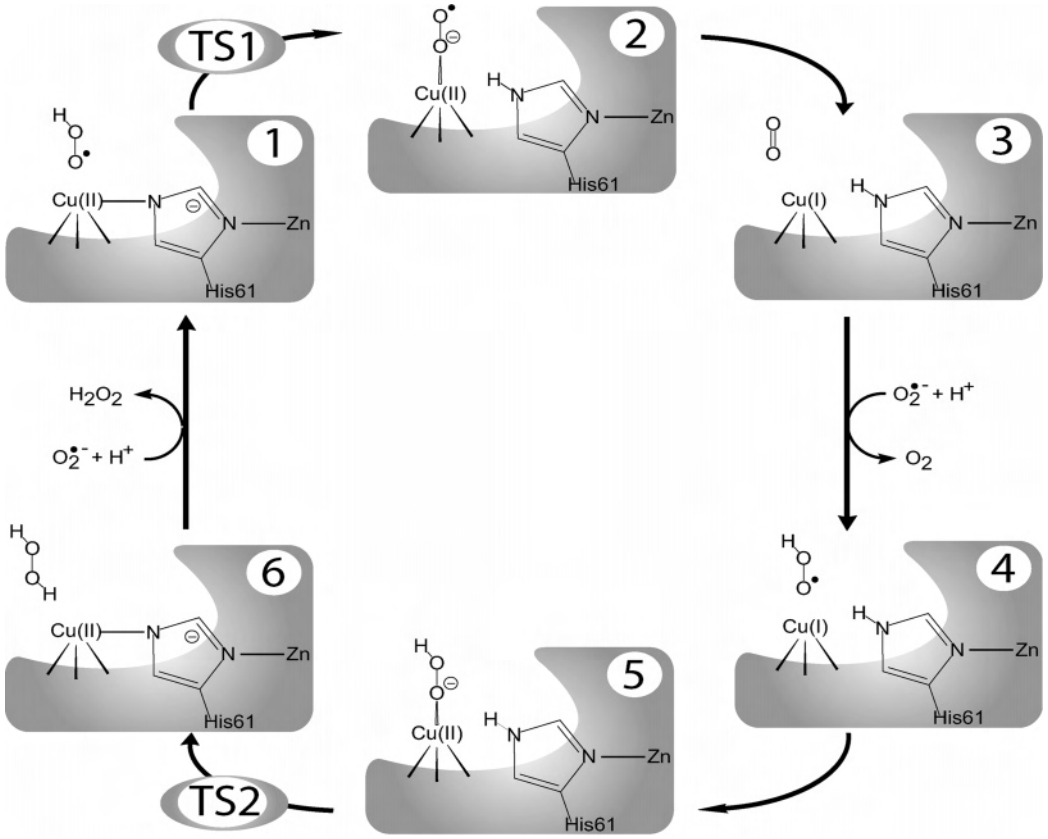

Figure 4. Presently investigated reaction mechanism for the dismutation by CuZnSOD.

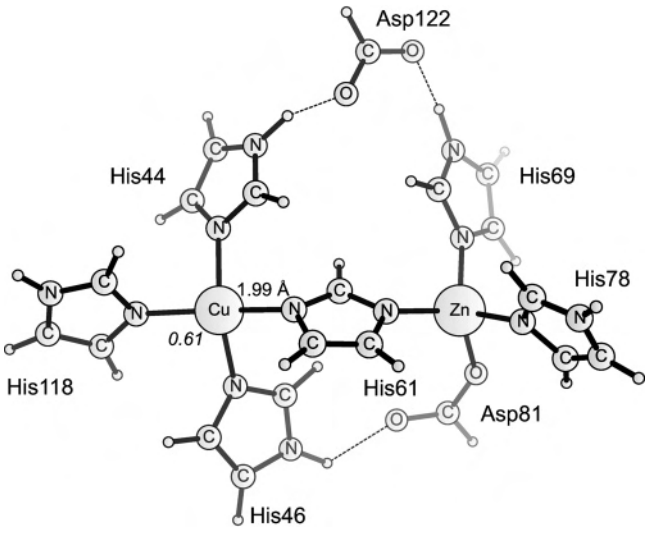

Figure 5. Oxidized Cu^{2+} resting cluster for states **1** and **6**. Important distances and spin populations are given.

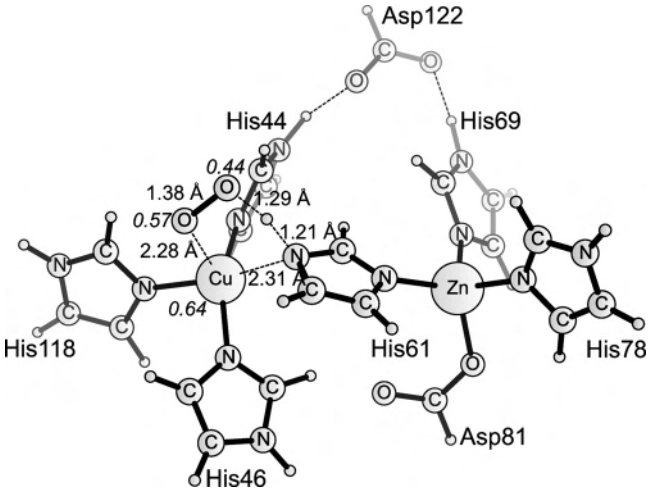

Figure 6. First transition state **TS1** involving the Cu-His61-Zn bridge rupture. Important distances and spin populations are given.

Information for the **1′** structure). The binding energy of $^{\bullet}$-OOH to the active site model is −6.2 kcal/mol, which is strongly destabilized by an entropy effect of 7.2 kcal/mol. The energy required to protonate $O_2^{\bullet-}$, solvent effects, and zero-point energy contributions further destabilize **1′** (the relative contributions to the Gibbs free energies for the different points are listed in Table 1). **1′** is 7.8 kcal/mol above **1**; therefore, the actual enzyme−substrate complex is not relevant here. The starting point **1** in fact describes the resting Cu^{2+} state cluster (see Figure 5) plus $O_2^{\bullet-}$ radical localized in the cavity.

The first transition state **TS1** involves substrate binding as a superoxide radical and His61 protonation, concomitantly with the Cu-His61-Zn bridge rupture at the copper side (see Figure 6). No metal reduction occurs at this stage. **TS1** involves motion of heavy atoms (Cu, N^{ϵ}_{His61}, and the substrate oxygens), and the corresponding imaginary frequency is relatively low (−266 cm^{-1}) (see the Supporting Information for the visualized vibration). The optimized transition state has an activation energy of 12.6 kcal/mol (see the Gibbs free energy profile in Figure 11), and this barrier is entropy-dominated. Without the entropy effects, **TS1** is only 2.3 kcal/mol above **1** (see Table 1). Another factor,

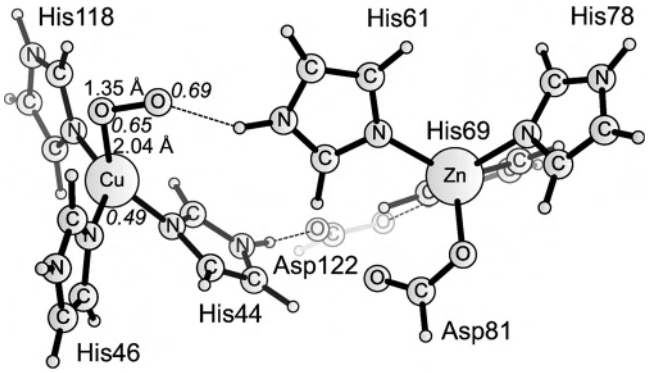

Figure 7. Intermediate **2** of the reductive phase with the superoxide radical anion bound to Cu^{2+}. Important distances and spin populations are given.

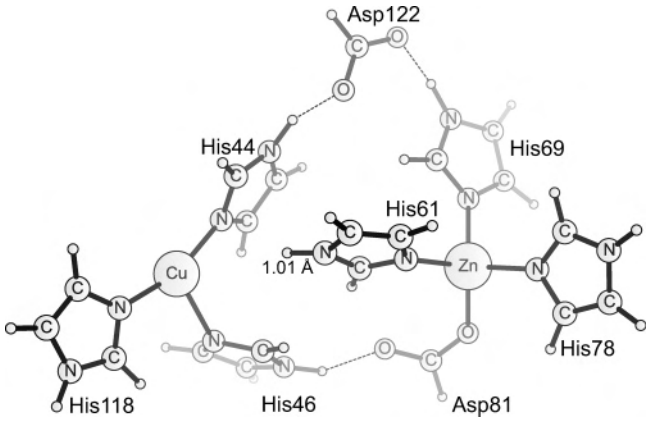

Figure 8. Reduced Cu^{+} cluster for states **3** and **4**. Important distances and spin populations are given.

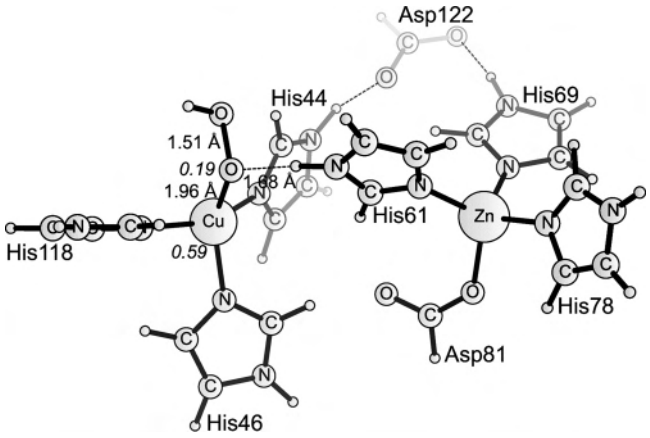

Figure 9. Intermediate **5** of the oxidative phase with the protonated peroxide anion bound to Cu^{2+}. Important distances and spin populations are given.

which increases the activation energy of **TS1** by 3.0 kcal/mol, is the normal state of the substrate (deprotonated $O_2^{\bullet-}$ superoxide anion, and not $^{\bullet}$OOH) at pH = 7, as described above.

As Cu^{2+} loses its N^{ϵ}_{His61} ligand, the emerging $O_2^{\bullet-}$ superoxide radical anion binds to Cu^{2+} (see Figure 7). Relative to the starting point **1**, intermediate **2** is exergonic by 18.4 kcal/mol. Formation of the dioxygen product and copper reduction to Cu^{+} results in state **3** (see Figure 8), which is endothermic by 2.7 kcal/mol relative to **2**, considering the enthalpies. The relative magnitude of the dielectric effects reaches its maximum of 7.3 kcal/mol at **3**, as compared to the starting point **1** (for $\epsilon = 80$, this value is 10.4 kcal/mol; see Table 1). This large effect is not surprising, knowing that the interaction of nonpolar O_2 with the protein medium is 5.0 kcal/mol weaker than the one of $^{\bullet}$OOH. Intermediate **2** is in a local minima only without the inclusion of the entropy effects. The entropy contribution of the dioxygen molecule release at **2** → **3** is −3.6 kcal/mol (see Table 1). The net result is that **2** and **3** are virtually degenerate on the potential energy surface (see Figure 11) with **2** above **3** by only 0.9 kcal/mol. Step **2** → **3** most probably occurs without any activation barrier. After the dioxygen molecule leaves, Cu^{+} attains a trigonal planar coordination with the three structural histidine ligands.

Thus the reductive half-reaction is essentially a single-step dioxygen formation, exergonic by 19.3 kcal/mol. As in eq 2, the products **3** of the reductive phase are the Cu^{+} spinless cluster and the triplet dioxygen molecule. The reductive phase **1**−**3** therefore occurs on the triplet spin surface. The calculated singlet−triplet splitting for intermediate **2** is 4.9 kcal/mol, favoring the high-spin state. Very similar geometries were obtained for the high- and low-spin states of **2**. Consideration of **TS1** as a singlet therefore would not stabilize this transition state.

ii. Oxidative Phase and H_2O_2 Formation. The dioxygen molecule formed during the reductive phase leaves the system at point **3** (see Figure 4). The second half-reaction starts from state **4** with the Cu^{+} cluster identical to **3** but with the second $^{\bullet}$OOH substrate radical inbound in place of O_2. In contrast to the weak substrate interaction with the resting Cu^{2+} cluster, the copper oxidation occurs spontaneously when the hydroperoxyl approaches the metal center, resulting in intermediate **5** (see Figure 9) with the $^{-}$OOH hydroperoxide anion bound to Cu^{2+}. The Cu−O distance is 1.96 Å in **5**, which is the shortest copper to substrate oxygen distance attained during the dismutation pathway. The redox binding **4** → **5** is strong enough to overcome the entropy factor of free $^{\bullet}$OOH: the free energy of **5** is −11.5 kcal/mol as compared to **4** and as much as −19.8 kcal/mol when the entropies are not considered. The pH factor stabilizing **4** by 3.0 kcal/mol is already included here.

The second and the last transition state **TS2** of the present mechanism (see Figure 10) involves formation of the hydrogen peroxide product using the proton from the N^{ϵ}_{His61} nitrogen. The favorable oxygen to nitrogen $O-N^{\epsilon}_{His61}$ hydrogen bonding is present already in **5**. **TS2** also involves concomitant Cu-His61-Zn bridge reformation. Similarly to **TS1**, the imaginary frequency of **TS2** is relatively low (-134 cm^{-1}) due to the involvement of heavy atom displacements (see the visualization in the Supporting Information section). Again as in **TS1**, there is no copper redox activity during **TS2**, but rather a change in the His61 protonation status. Starting from the preceding intermediate **5**, **TS2** has an activation energy of 17.6 kcal/mol.

The final state **6** is the oxidized Cu^{2+} cluster equivalent to the initial state **1**, plus a H_2O_2 molecule localized inside the active site channel. The hydrogen peroxide molecule formed in **TS2** has a very small enthalpic binding energy,

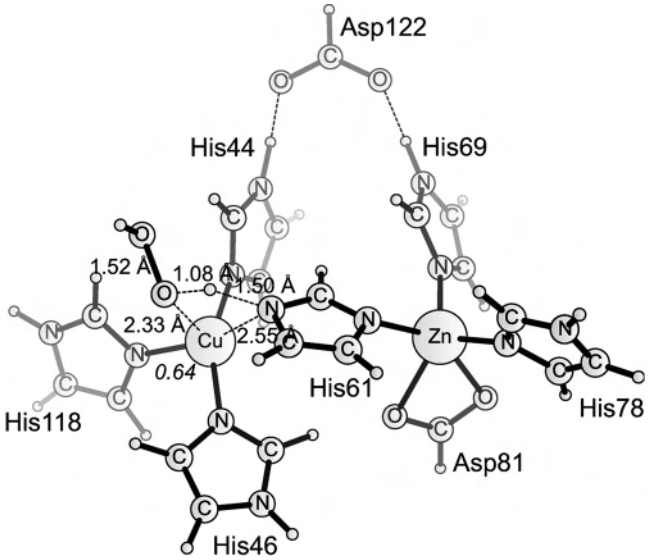

Figure 10. Second transition state **TS2** involving the Cu-His61-Zn bridge reconstruction and H_2O_2 formation. Important distances and spin populations are given.

and this binding is further destabilized by 6.5 kcal/mol of entropy. The optimized state **6′** with H_2O_2 loosely bound has a copper to oxygen distance of 2.73 Å (see the Supporting Information for the **6′** structure). The relative contributions to the energy of **6′** versus **6** are very similar to the energy components of **1′** versus **1** (excluding the ΔG_{OOH} factor) (see Table 1). Similar to **1′**, the **6′** state is also metastable, lying 2.4 kcal/mol above **6**.

The oxidative half-reaction **4**−**6** is (similar to the reductive part **1**−**3**) essentially a single-step process with an exergonicity of 4.9 kcal/mol, occurring on the doublet spin surface. In contrast to the absence of bound states during the reductive phase, state **5** here is a stable intermediate.

III.c. Importance of Asp122. The negatively charged Asp122 carboxylate links the His44 and His69 metal ligands via hydrogen bonding. Among the active site residues, Asp122 was also proposed to contribute most significantly to the CuZnSOD pK_a value, shifting it upward by $\Delta pK_a = 4.6$ units.[22,23] The role of Asp122 can be estimated by removal of its formate equivalent from our model in Figure 3 and performing a reoptimization of the points obtained initially for the full system. The charge of the Asp122-deficient model is +2 units. For a brief analysis, the thermochemical corrections were approximated from the full model discussed above.

Structurally, the cupric Cu^{2+} states **1** (or equivalently **6**), **2**, **TS1**, **TS2**, and **5** show no considerable rearrangements upon the reoptimization. For Asp122-present and -deficient models, state **1** in fact provides a good reference for the X-ray structural data on the enzyme resting state (see Table 2). In accordance, for the oxidized copper states there is no significant deviation in the relative energies between the values discussed previously and the Asp122-deficient model. In contrast, for the cuprous Cu^+ cluster **3** (or equivalently **4**) the conformation drastically changes. The protonated N^{ϵ}_{His61} nitrogen of the bridging histidine moves ∼5 Å away from Cu^+, and the Cu−Zn internuclear distance increases

Table 2. Structural Parameters for the Resting Oxidized Cu^{2+} (Intact Cu-His61-Zn Bridge) and Protonated Reduced Cu^+ (Broken Cu-His61-Zn Bridge) States as Obtained in the Present and Earlier Model Calculations as Compared to the X-ray Crystallography Data[a]

	Cu−N^{ϵ}_{His61} (Å)		Cu−Zn (Å)	
state and its present notation	X-ray	model with Asp122 present/absent	X-ray	model with Asp122 present/absent
Cu^{2+} or **1**(**6**)	2.2[b]	1.99/2.02, 2.04[d]	6.0−6.2[b]	5.86/5.98, 5.91[d]
Cu^+ or **3**(**4**)	3.0,[b] 3.3[c]	4.09/9.17, 3.39[d]	6.9[c]	7.78/10.92, 6.66[d]

[a] Models with the Asp122 present and absent are considered. [b] Distances from different structures, averaged to 0.1 Å.[9,24] [c] Distances from the recently obtained high 1.15 Å resolution structure[24] of the reduced dimeric CuZnSOD. [d] Distances from the model calculations using the VBP density functional.[22]

by ∼2 Å (see Table 2). The N^{ϵ}_{His44} and N^{ϵ}_{His69} nitrogens are no longer bridged by Asp122, and the N^{ϵ}_{His44}−N^{ϵ}_{His69} internuclear distance extends to ∼16 Å, as compared to ∼5 Å for the reduced copper state in the Asp122-present model. This large increase of more than 10 Å is, of course, not likely in an enzyme but gives an indication of the strength of the forces. The difference in behavior of the Asp122-deficient system for the Cu^{2+} and Cu^+ states comes from the metal coordination geometry in these states: distorted square planar for Cu^{2+} and trigonal planar for Cu^+. Due to the relaxation, states **3** and **4** receive a relative stabilization of 6.2 kcal/mol. This increases the exergonicity of the reductive half-reaction to 25.5 kcal/mol but simultaneously turns the energetic effect of the oxidative half-reaction into an endergonicity of 1.3 kcal/mol, The equilibrium under such condition is shifted to the left, and the Asp122-deficient enzyme could probably catalyze the reverse reaction of the normal oxidative phase. The **6** → **TS2** reversal of the second half-reaction for the modified model has a moderate activation energy of 14.9 kcal/mol. This activity would be reflected in consumption of hydrogen peroxide and production of superoxide radical anions. This side action of Asp122 elimination possibly illustrates its importance for the enzyme. The production of $O_2^{\bullet-}$ by the mutant CuZnSOD has actually been proposed earlier[60,61] based on experiments. $O_2^{\bullet-}$ production is often related[5] to the toxic activity of the FALS-associated CuZnSOD mutants.

III.d. Reaction Energetics. The experimental values for the reduction potentials $E^{\circ\prime}(O_2/O_2^{\bullet-}) = -160$ mV and $E^{\circ\prime}(O_2^{\bullet-}/H_2O_2) = +890$ mV,(see section I) give a total reaction energy of −24.2 kcal/mol (see eq 7). The currently obtained overall energy of −19.3−4.9 = − 24.2 kcal/mol thus appears to be in perfect agreement with the experimental data. The energetics of the individual reductive and oxidative phases can be calculated, considering the above given $E^{\circ\prime}$ values together with the redox potential $E^{\circ\prime}(Cu^{2+}/Cu^+)$ in CuZnSOD, reported to range between +120 and +420 mV. This corresponds to the reductive phase being exergonic by 6.7−13.4 kcal/mol and the oxidative phase

(60) Beckman, J. S.; Estewez, A. G.; Crow, J. P.; Barbeito, L. *Trends Neurosci.* **2001**, *24*, S15−S20.
(61) Estewez, A. G.; Crow, J. P.; Sampson, J. B.; Reiter, C.; Zhuang, Y.; Richardson, G. J.; Tarpey, M. M.; Barbeito, L.; Beckman, J. S. *Science* **1999**, *286*, 2498−2500.

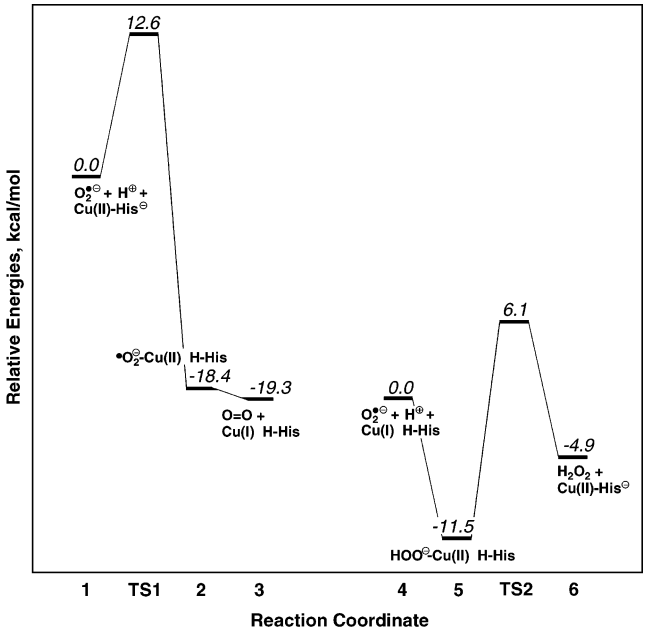

Figure 11. Free energy profile obtained for the catalysis by CuZnSOD using $\epsilon = 4$ for the solvent effects. Individual contributions to the free energy values are given in Table 1. Metastable states **1′** and **6′** were left out from the profile.

being exergonic by 10.8−17.8 kcal/mol. The presently obtained values are at least 5.9 kcal/mol offset and would imply $E^{\circ\prime}(Cu^{2+}/Cu^{+}) = 680$ mV outside the experimental data range. A possible problem with the present model is the underestimation of the polarity of the active site environment with a dielectric constant $\epsilon = 4$. Reexamination of the potential energy surface with $\epsilon = 80$ (corresponding to water) results in the reductive and oxidative phases being exergonic by 16.2 and 6.2 kcal/mol, respectively (see Table 1), providing a somewhat better agreement with the experimental $E^{\circ\prime}(Cu^{2+}/Cu^{+})$ values for CuZnSOD. The major contribution to the difference in the relative solvent energies at different values of ϵ is, however, due to the contributions from the reagent and product molecules: going from $\epsilon = 4$ to $\epsilon = 80$ does not make any considerable effect on E_{SOLV} for O_2 but gives the additional −2.6 kcal/mol for •OOH and −3.4 kcal/mol for H_2O_2. State **2** becomes stable within the highly polar environment, but its stability by 1.5 kcal/mol as compared to **3** is only marginal.

Examination of the free energy surface for the dismutation process (see Figure11) shows that the first half-reaction is irreversible due to the very high **3** → **TS1** activation barrier of 31.9 kcal/mol. On the other hand, the **6** → **TS2** reversal of the second half-reaction has a much smaller activation energy of 11.0 kcal/mol, and this reversal therefore appears possible. Indeed, there exist experimental observations of CuZnSOD interaction with H_2O_2 leading to inactivation,[62] but reactions of the wild-type enzyme with O_2 were not observed to the best of our knowledge. The inactivation was caused by a mutation of one histidine at the active site[63,64] and was proposed to start from the Cu^{2+} state:[62,65]

$$E\text{-}Cu^{2+} + H_2O_2 \rightleftarrows E\text{-}Cu^{+} + O_2^{\bullet-} + 2H^{+} \quad (8)$$

$$E\text{-}Cu^{+} + H_2O_2 \rightleftarrows E\text{-}Cu^{2+}\text{-}{}^{\bullet}OH + {}^{-}OH \quad (9)$$

$$E\text{-}Cu^{2+}\text{-}{}^{\bullet}OH + H\text{-}His\text{-}E \rightarrow E\text{-}Cu^{2+} + {}^{+\bullet}His\text{-}E + {}^{-}OH \quad (10)$$

During the first step, the copper reduction and $O_2^{\bullet-}$ production occurs, which is similar to the reversal of the normal reaction path. The second H_2O_2 oxidizes the metal center and leads to a strongly bound Cu^{2+}-•OH oxidant, supported by data on H_2O_2 conversion to hydroxyl radical by CuZnSOD.[66] This oxidant finally oxidizes a nearby histidine and thereby inactivates the enzyme. The straightforward candidate for the histidine in eq 10 is His61. Using a similar modeling as in the present study, CuZnSOD inactivation can be a topic of a separate theoretical investigation.

IV. Conclusions

Superoxide dismutation by CuZnSOD has been investigated using quantum chemical methods. An important assumption of this study is a tightly linked delivery of protons and superoxides to the catalytic copper center, so that the immediate substrate at the active site is a neutral •OOH hydroperoxyl radical. This is advantageous from a modeling point of view (see section III.b and previous studies[54]) and allows the charge of the model to be kept constant during the reaction. As described in section I, electrostatic attraction plays an important role in the affinity of anionic $O_2^{\bullet-}$ superoxides to the active site. However when the $O_2^{\bullet-}$ substrate radical penetrates into the active site channel and approaches the copper center, it can be protonated on its way by a proton donor similarly as proposed for NiSOD.[58] It has been stressed that SOD enzymes scavenge $O_2^{\bullet-}$ and thereby preclude •OOH radical formation, which is likely to initiate peroxidation and autoxidation of the cell membrane lipids.[67,68] In view of the present results, the SOD active site provides a safe device to protonate $O_2^{\bullet-}$ and then immediately disproportionate it. This is in line with the idea that a number of processes in oxidative biochemistry are better understood when considering hydroperoxyl radical involvement.[69] To consider the superoxide radical being protonated (pK_a(OOH) = 4.8) at neutral acidity (pH = 7), the current approach includes correction to the relative energies (see sections II and III.b). Another important factor influencing the energetics is the entropic contribution, known to be far from obvious in enzyme catalysis.[53,70] Translational entropies were estimated here considering reactant and product molecules

(62) Hodgson, E. K.; Fridovich, I. *Biochemistry* **1975**, *14*, 5294−5298.
(63) Bray, R. C.; Cockle, S. H.; Fielden, E. M.; Roberts, P. B.; Rotilio, G.; Calabrese, L. *Biochem. J.* **1974**, *139*, 43−48.
(64) Blech, D. M.; Borders, C. L., Jr. *Arch. Biochem. Biophys.* **1983**, *224*, 579−586.
(65) Liochev, S. I.; Fridovich, I. *Proc. Natl. Acad. Sci. U.S.A.* **2004**, *101*, 743−744.
(66) Yim, M. B.; Chock, P. B.; Stadtman, E. R. *Proc. Natl. Acad. Sci. U.S.A.* **1990**, *87*, 5006−5010.
(67) Yamaguchi, K. S.; Spencer, L.; Sawyer, D. T. *FEBS Lett.* **1986**, *197*, 249−252.
(68) Salvador, A.; Sousa, J.; Pinto, R. E. *Free Radical Biol. Med.* **2001**, *31*, 1208−1215.
(69) De Grey, A. D. *DNA Cell Biol.* **2002**, *21*, 251−257.
(70) Villa, J.; Strajbl, M.; Glennon, T. M.; Sham, Y. Y.; Chu, Z. T.; Warshel, A. *Proc. Natl. Acad. Sci. U.S.A.* **2000**, *97*, 11899−11904.
(71) Humphrey, W.; Dalke, A.; Schulten, K. *J. Mol. Graphics* **1996**, *14*, 33−38.

blocked inside the active site cavity (see section II) in contrast to gas-phase values.

The catalytic cycle consists of two half-reactions with only a single substrate molecule interacting with the copper center for each half-reaction. The first half-reaction is the reductive phase, involving reduction of the resting Cu^{2+} cupric form followed by dioxygen product formation (see eq 2). During the second half-reaction, the Cu^{+} cuprous center is oxidized back to its initial state, and the hydrogen peroxide product is released (see eq 3). As described in section I, the reduction is predicted to occur via inner sphere electron transfer with direct $O_2^{\bullet-}$ coordination to the Cu^{2+} metal center. On the other hand, the interpretation of the FTIR analysis[34] suggests that the oxidative phase occurs via outer sphere electron transfer without direct coordination of $O_2^{\bullet-}$ to Cu^{+}. Consistently, we do not observe substrate binding to the reduced Cu^{+} center. In the present scheme, oxidative coordination to Cu^{+} is found, and the actual bound state **5** is for the oxidized Cu^{2+} cluster. Not contradicting the FTIR experiment but in contrast to its earlier interpretation, both the reductive and oxidative half-reaction here involve the direct contact of the substrate with copper and formation of a transient $O^{-}-Cu^{2+}$ bond. Anionic species bound to the metal center are the $O_2^{\bullet-}$ superoxide (state **2**, Figure 7) and the $^{-}$OOH hydroperoxide anion (state **5**, Figure 9) in the first and second phase, respectively. The intermediate **2** of the reductive phase is virtually degenerate with products **3** (see Figure 8), and the only stable intermediate of the catalytic cycle is state **5**. Reactants (**1** and **4**) and products (**3** and **6**) are unbound states (see Figure 4), strongly stabilized by entropy (see Table 1) as compared to the intermediates and transition states.

Cu,Zn clusters of **1**(**6**) and **3**(**4**) correspond to the experimentally observed resting oxidized Cu^{2+} and protonated reduced Cu^{+} CuZnSOD states, respectively. For the reduced state with the protonated Cu-His61-Zn bridge, the present modeling suggests Asp122 carboxylate to be essential in the active site stabilization (see section III.c and the comparison to the X-ray data in Table 2). When optimized in a vacuum, the Asp122-deficient model with the positive charge of +2 units displays unrealistic expansion. Interestingly, a better structural correlation with the X-ray data for the reduced state was found during the earlier theoretical modeling,[22] lacking Asp122. This modeling however included a water molecule, forming the hydrogen bonding bridge between the protonated N^{ϵ}_{His61} nitrogen and one of the copper-coordinated nitrogens (N^{δ}_{His44}, N^{ϵ}_{His46}, or N^{ϵ}_{His118}).

The presently obtained overall dismutation energetics is in perfect agreement with the actual reduction potentials $E^{\circ\prime}(O_2/O_2^{\bullet-})$ and $E^{\circ\prime}(O_2^{\bullet-}/H_2O_2)$. With a dielectric constant $\epsilon = 4$, individual reduction and oxidation half-reactions energies are about 6.0 kcal/mol offset (5.9 kcal/mol larger for the reductive phase and 5.9 kcal/mol smaller for the oxidative phase) from the values calculated from the experimental data range on $E^{\circ\prime}(Cu^{2+}/Cu^{+})$. Recalculation of solvent effects in the highly polar environment with $\epsilon = 80$ slightly improves the correlation with the experimental data (see section III.d).

The transition states **TS1** (Figure 6) and **TS2** (Figure 10) do not involve copper redox activity, but rather Cu-His61-Zn bridge protonation/deprotonation concomitant with its rupture/reformation at the copper side. Redox processes at the Cu center (reduction **2** → **3** and oxidation **4** → **5**) occur without apparent activation barriers. The free energy activation barriers of **TS1** and **TS2** are 12.7 and 17.6 kcal/mol, respectively (13.7 and 17.0 kcal/mol when $\epsilon = 80$). The difference between these two values is within the error bars of the method, considering the approximate procedures to include entropy and estimate the local pH influence. This is consistent with kinetic data[30] showing equal rates for the oxidized and reduced CuZnSOD forms. The reported turnover number is $k_{cat} \approx 1 \times 10^6\ s^{-1}$,[15] and taking into account the absence of Arg141 in the model (see section I), the rate-limiting step should be 10.7 kcal/mol high. Averaged between the energies for **TS1** and **TS2**, the currently suggested activation barrier is around 15 kcal/mol, which is satisfactory given the uncertainties listed above.

Acknowledgment. The National Supercomputer Center (NSC) in Linköping is gratefully acknowledged for a generous grant of computer time. We thank Prof. Louis Noodleman for valuable discussions.

Supporting Information Available: GIF file showing the first transition state **TS1** of the CuZnSOD mechanism, a visualized vibration that depicts the Cu-His61-Zn bridge protonation and corresponds to the imaginary frequency of $-266\ cm^{-1}$; GIF file showing the second transition state **TS2** of the CuZnSOD mechanism, a visualized vibration that depicts the Cu-His61-Zn bridge re-formation and corresponds to the imaginary frequency of $-134\ cm^{-1}$; chart depicting two metastable complexes (1′ and 6′, respectively) in which $^{\bullet}OOH/H_2O_2$ weakly bind to Cu^{2+}/Cu^{2+} model clusters. This material is available free of charge via the Internet at http://pubs.acs.org.

IC050018G